Published February 3, 2015

The Use of Electromagnetic Induction to Monitor Changes in Soil Moisture Profiles beneath Different Wheat Genotypes

Peter W. Shanahan
Andrew Binley*
Lancaster Environment Centre
Lancaster Univ.
Lancaster, LA1 4YQ
United Kingdom

W. Richard Whalley
Christopher W. Watts
Rothamsted Research
Harpenden, AL5 2JQ
United Kingdom

There has been recent interest in the use of surface-deployed geophysical methods to estimate soil moisture profiles. In this study, we applied multi-coil, frequency domain, electromagnetic induction (EMI) geophysical surveys to determine electrical conductivity (σ) profiles of the root zone of four winter wheat (*Triticum aestivum* L.) genotypes grown in a randomized block experiment with four replicates. Field measurements of apparent electrical conductivity (σ_a) were obtained at sites with two different soil textures. We used the cumulative sensitivity model to predict EMI conductivity data from the conductivity profile measured with electrical resistivity tomography (ERT) on a subset of the plots we investigated. During the inversion of the EMI data, conductivities were adjusted on all plots so that they were consistent with the ERT data. Changes in electrical conductivity of field soil, with depth computed from inversion of the EMI data, during the growth period were compared with measured changes in soil water content. Laboratory measurements confirmed a positive correlation between electrical conductivity and soil water content. Between crop emergence and maturity, water extraction by the different wheat genotypes reduced the water content by up to 30% Comparing changes in electrical conductivity between reference profiles determined shortly after crop emergence and electrical conductivity profiles at later dates as the crop matured, we were able to use EMI to remotely monitor moisture extraction by the roots of different wheat genotypes with depth and time.

Abbreviations: CS, cumulative sensitivity; EMI, electromagnetic induction; ERT, electrical resistivity tomography; McMC, Markov chain Monte Carlo.

Rapid assessment of crop phenotypic traits (e.g., root architecture, leaf area index) is an important requirement for plant breeders (Araus and Cairns, 2014; Dodd et al., 2011). Repeated measurement of soil moisture profiles may provide a method to infer root activity as a function of depth. Below the surface, root proliferation and architecture determine water extraction from the soil (Bengough et al., 2011). Traditional methods to measure soil moisture profiles include: auger samples, bulk density tins, buried sensors (e.g., time domain reflectometry or frequency domain sensors) or sensors that use access tubes (e.g., neutron probes). These methods are invasive and labor intensive for repeated observations and only provide limited spatial resolution. The cost of buried sensors can become prohibitive when the number of plots becomes large. In some cases (auger samples or neutron probes), the temporal resolution is poor. Geophysical methods have been applied to large-scale mapping of soil properties, including: soil

Soil Sci. Soc. Am. J. 79:459–466
doi:10.2136/sssaj2014.09.0360
Open access article.
Received 9 Sept. 2014.
Accepted 11 Dec. 2014.
*Corresponding author (a.binley@lancaster.ac.uk).

water content, soil water salinity, soil texture, and soil organic matter content (Corwin and Lesch, 2005). Geophysical methods applied to agricultural studies include: electrical resistivity tomography (ERT) (e.g., Binley and Kemna, 2005); electromagnetic induction (EMI) (e.g., Brevik et al., 2006; von Hebel et al., 2014); and ground-penetrating radar (Vanderborght et al., 2013). In this study, we used ERT and EMI techniques to map the soil electrical conductivity (σ) to infer soil drying profiles beneath winter wheat.

An increase in soil water content generally increases the soil electrical conductivity (σ) for a given porosity and texture (Archie, 1942). Soil σ is also a function of the pore fluid electrical conductivity and temperature (Corwin and Lesch, 2005). Electrical resistivity tomography has been used to study the variation of soil electrical conductivity in the root zone (Srayeddin and Doussan, 2009; Furman et al., 2013). It is best suited for use in electrically resistive environments such as dry soil. The disadvantage for agricultural applications is the requirement for galvanic contact between electrical probes and the soil, resulting in a disturbed soil surface and extensive electrical cabling. In contrast, EMI measures apparent electrical conductivity (σ_a) noninvasively by inductive coupling (e.g., Mester et al., 2011), without the need for contact with the soil surface. It is a quick and repeatable measurement method that can be used at the field and plot scales (Vereecken et al., 2014). Electromagnetic induction instruments measure σ_a, and this represents the weighted average of the soil σ across a depth range that depends on the separation distance (*s*) between the transmitter and receiver coils as well as their orientation (McNeill, 1980). When *s* is increased, the depth of soil contributing to the σ_a measurement increases (e.g., McNeill, 1980; Callegary et al., 2007). Given a set of σ_a measurements obtained with different coil spacings and orientations, a vertical profile of soil conductivity can be estimated through inverse modeling (Mester et al., 2011; von Hebel et al., 2014). Examples of EMI instruments applied to soil science include the EM-38, containing a single receiver coil in earlier models and a pair of receiver coils in the more recent MK2 version (Geonics Ltd.), the Dualem, which has two receiver coils (Dualem), and the CMD Explorer and Mini-Explorer, which have three receiver coils (GF Instruments).

A comparison of EMI measurements between two points in time makes it possible to separate the contributions of temporally dynamic soil properties (e.g., water content and pore water electrical conductivity) from the contribution of temporally stable soil properties (e.g., texture) (Vereecken et al., 2014). So-called EMI time lapse can be used as a tool to observe changes in soil conductivity profiles in the root zone (Cassiani et al., 2012) with a view to making inferences about changes in water content profiles. There are two general approaches to invert EMI data: the first is based on the cumulative sensitivity (CS) approach (McNeill, 1980); the second is based on a solution to the Maxwell equation (Mester et al., 2011). In this study, we adopted the CS approach because of its widespread use, its simplicity, and the computational efficiency of the resulting inverse model.

Our aim was to assess whether EMI measurements can provide a method to determine changes in soil moisture as a function of depth under growing crops. We studied four winter wheat genotypes grown on two field sites with different soil textures. Our objectives were: (i) to explore the use of EMI as a method to measure electrical conductivity–depth profiles that develop as a result of soil drying by roots of wheat; and (ii) to develop an approach to allow time-lapse data to be interpreted with simple functions, thus allowing a comparison between profiles of soil water extraction by different winter wheat genotypes.

METHODOLOGY

Soils and Field Site Data

In this study, we used two experimental field sites, Butt Close and Warren Field, located near Woburn, Bedfordshire, UK. Butt Close consists of a sandy loam soil and Warren Field a silty clay loam soil (Table 1). Both sites are managed by Rothamsted Research. At a depth of approximately 40 cm on Butt Close there is a cemented layer, and beneath that there is almost pure sand. The vertical gradient in texture at Warren Field is negligible; however, the surface layer (approximately 30 cm) has a higher organic matter content and is less dense.

Table 1. Description of site and soil properties of Butt Close and Warren Field, Woburn Experimental Field Station, Bedfordshire, UK (adapted from Whalley et al., 2012).

Property	Butt Close	Warren Field
Location	52°0′42″ N, 0°32′42″ W	52°1′6″ N, 0°35′30″ W
Soil type		
SSEW† group	Brown Earth	Brown Earth
SSEW series	Cottenham	Flitwick
FAO	Cambric Arenosol	Dystric Cambisol
Sand (2000–65 μm), kg kg^{-1} dry soil	0.88	0.54
Silt (63–2 μm), kg kg^{-1} dry soil	0.06	0.20
Clay (<2 μm), kg kg^{-1} dry soil	0.07	0.26
Texture (SSEW class)	loamy sand	sandy clay loam
Particle density, g cm^{-3}	2.65	2.59
Organic C, kg kg^{-1} dry soil	0.01	0.04

† SSEW, Soil Survey of England and Wales.

The experiment was fully randomized in four blocks. Each block contained 23 wheat genotypes and a fallow (uncultivated) plot, in plots 1.8 m wide and 7.0 m long, to give a total of 24 plots per block. Both sites had the same experimental design but with a different randomization of the position of each wheat genotype. For this study, we analyzed four contrasting wheat genotypes: (i) Mercia winter wheat carrying an introgressed Rht-B1c (formerly Rht3) allele, hereafter named Dwarf wheat; (ii) Hystar hybrid wheat (Saaten-Union Gmbh), hereafter named Hystar; (iii) Xi19 (Limagrain UK Ltd.); and (iv) Robigus (KWS UK Ltd.), using data collected from May to August in the 2013 growing season. The wheat was sown in

early March 2013. Gravimetric soil water content (θ_g) was determined from auger samples taken at 0.1-m depth intervals to the 1.0-m depth for all plots of the four wheat genotypes selected for this study. These measurements coincided with ERT and EMI measurements (see below) taken on approximately 16 May, 14 June, 21 June, 28 June, 9 July and 1 Aug. 2013 (exact dates for each site are indicated below).

Calibration of Water Content and Electrical Conductivity

In the laboratory, σ and volumetric water content (θ_v) were measured on samples of both soils to establish a relationship between these properties. Electrical conductivity was measured on repacked samples in three 5.3-cm-diameter and 4-cm-long cores from each soil. A four-electrode arrangement, with electrodes connected to a resistance meter (RM4, from Geoscan) was used to measure electrical conductivity. Volumetric water content was measured on a separate soil sample using a SM150 dielectric soil moisture sensor (Delta-T Devices Ltd.) connected to a datalogger. All of the cores were placed in a pressure plate apparatus, which was used to apply step changes in matric potential between 0.5 and 450 kPa. Before the start of the calibration, the soil samples were saturated with 0.05 mol L^{-1} NaCl, and the water content and electrical conductivity were recorded at equilibrium water contents.

Electrical Resistivity Tomography

Electrical resistivity tomography measurements were made at both field sites on two of the four blocks. These data were later used to assist with analysis of the EMI data (see below). We used four 96-electrode arrays. Each array had electrodes measuring 0.1 m in length and 0.01-m diameter, inserted into the soil with 0.32-m separation, to give a 30.7-m-long array. A Syscal Pro electrical resistivity meter (Iris Instruments) was used to measure the apparent electrical resistivity (ρ_a) in a dipole–dipole electrode configuration to a maximum of eight levels (see, for example, Binley and Kemna, 2005). These data were checked for reciprocity of measurements (Parasnis, 1988) and then inverted to give a two-dimensional distribution of soil resistivity using the Occam's based R2 (Version 2.7a) ERT inverse code (Binley, 2013).

Electromagnetic Induction

We used a CMD Mini-Explorer (GF Instruments) EMI instrument to make measurements of σ_a at three positions along the center line of the experimental plots (Fig. 1a). The instrument is 1.3 m long and has a 30-kHz transmitter coil and three receiver coils at different spacings (s) from the transmitter (Fig. 1b; 0.32, 0.71, and 1.18 m). The probe can be rotated by 90° (about the long axis) to orient the coils in a horizontal coplanar (HC) or a vertical coplanar (VC) position. The different coil spacings and orientations allow six measurements of σ_a to be made at a single position on the plot. From here on, we refer to an EMI measurement configuration as XCY, where X is either H, for horizontal coplanar, or V, for vertical coplanar, and Y is 1, 2, or 3 to indicate

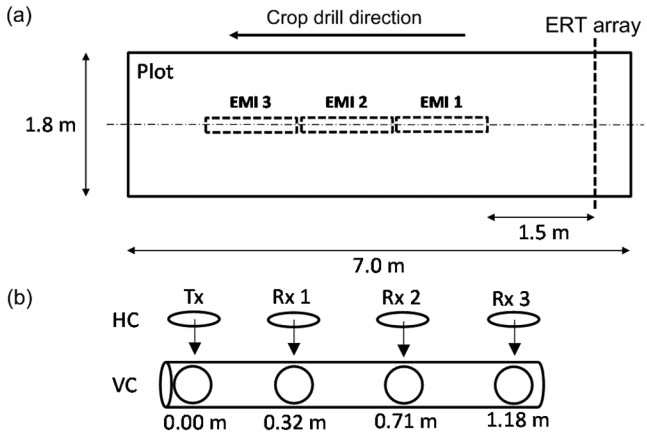

Fig. 1. (a) The layout of an experimental plot indicating the position of three electromagnetic induction (EMI) measurements taken in the center of the plot relative to the electrical resistivity tomography (ERT) array, which extends across adjacent plots; (b) the EMI instrument has one transmitter coil (Tx) and three receiver coils (Rx) and can be rotated through 90° to obtain vertical coplanar (VC) or horizontal coplanar (HC) measurements.

the coil spacing according to Fig. 1. The effect of different coil spacings and orientations is to modify the volume of soil that influences the conductivity measurements made by the EMI instrument, with HC3 providing the greatest volume (and depth) of soil sensed by the receiver. The cumulative sensitivity function (McNeill 1980) for vertical coplanar orientation is given by

$$CS(z)=\left[4\left(\frac{z}{s}\right)^2+1\right]^{1/2}-2\left(\frac{z}{s}\right) \quad [1]$$

and for horizontal coplanar orientation is given by

$$CS(z)=\left[4\left(\frac{z}{s}\right)^2+1\right]^{-1/2} \quad [2]$$

where z is depth and s is the coil separation. They are plotted in Fig. 2 for the CMD Mini-Explorer.

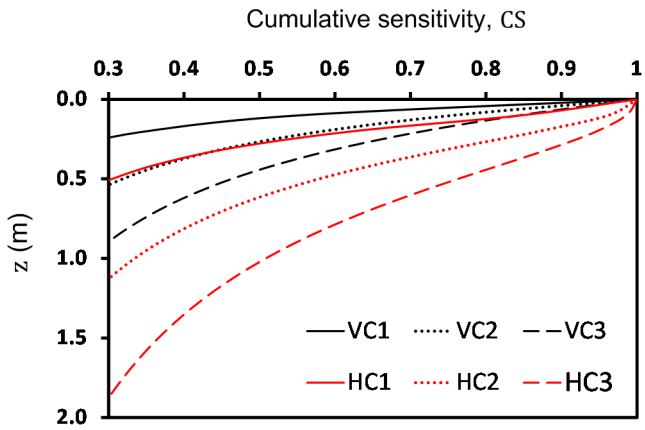

Fig. 2. Cumulative sensitivity (CS) profiles (0.3–1) for the CMD Mini-Explorer in vertical coplanar (VC) and horizontal coplanar (HC) modes. Coil separations are: 1 = 0.32 m, 2 = 0.71 m, and 3 = 1.18 m. The point where CS crosses the *y* axis indicates the effective depth (*z*) of measurement of the coil separation.

Before the field campaign, we developed a measurement protocol to minimize the effects of instrument drift. On each measurement occasion, the instrument was allowed to equilibrate to ambient temperatures for at least 1 h. A single location at each site, away from the plots, was monitored and established as a "drift base," where the probe could be returned periodically during each day to assess for any instrument drift (Corwin and Lesch, 2005). These assessments of instrument drift were then used to adjust all σ_a measurements. A measurement period of 1.0 s provided σ_a values with a reasonably low variability (root mean square error typically <2% for most soil conditions). The probe was kept 1.5 m from any metallic items (e.g., electrical cables) to prevent interference. To avoid any potential "operator effects," the same person used the instrument throughout the study.

Predicting Electromagnetic Induction Data from Soil Profile Conductivities Measured with Electrical Resistivity Tomography

We used the ERT data to predict the apparent electrical conductivities of the soil within the centers of plots as measured with the Mini-Explorer instrument in the six receiver configurations. These predictions were based on the different CS functions for the different probe configurations (Fig. 2; Eq. [1] and [2]) and determined from

$$\sigma_{aERT} = \sum_{i=1}^{n} \sigma_{ERTi} \left[CS(z_{i-1}) - CS(z_i) \right] \qquad [3]$$

where σ_{ERTi} are those electrical conductivity values inverted from the ERT data at depth $(z_{i-1} + z_i)/2$ and CS is the appropriate cumulative sensitivity function of McNeill (1980) for the particular coil configuration. Thus, σ_{aERT} values represent predictions of σ_a data measured with EMI. In our study, such data were available on two of the four blocks, allowing regressions to be obtained between the six measured conductivities for each EMI probe configuration and those predicted using the ERT data.

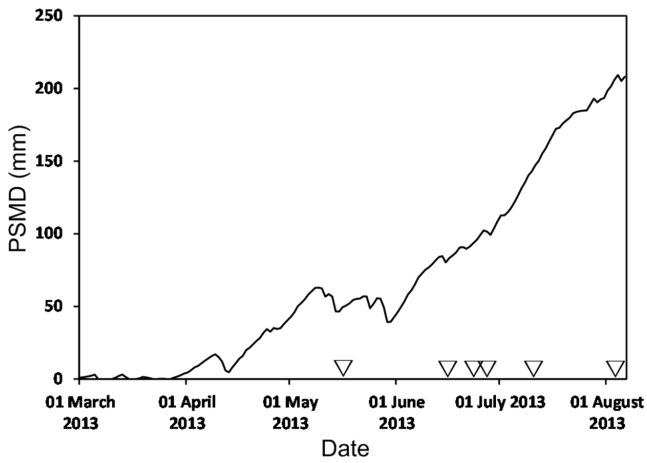

Fig. 3. Potential soil moisture deficit (PSMD) from meteorological data at Woburn Farm for the period of the study. Arrows indicate when measurements were made.

Inversion of Apparent Electrical Conductivity Data from Electromagnetic Induction

Before any inversion of the EMI data, we first adjusted the six EMI conductivity measurements so that they matched those predicted using ERT data as described above (as in Lavoué et al., 2010). The inversion on these data was conducted with a Bayesian Markov chain Monte Carlo (McMC) search-based algorithm model based on JafarGandomi and Binley (2013). The inversion for each position within the field plots (Fig. 1a) was conducted assuming a one-dimensional $\sigma(z)$ model. The inversion used the McNeill (1980) cumulative sensitivity forward model (Eq. [1–3]). Search limits for the inversion were set using the mean, minimum, and maximum σ_a values for each date of site surveys, as recommended by Mester et al. (2011).

The inversion reports a posteriori estimates of $\sigma(z)$ across a vertical profile of 2 m discretized into a minimum of two and maximum of three layers. Inversions were run for 20,000 iterations to achieve convergence. Conductivity values were then adjusted to a standardized temperature of 25°C (Campbell et al., 1949) to allow direct comparisons to be made between different dates.

RESULTS AND DISCUSSION

Soil and Site Characteristics

The potential soil moisture deficit (PSMD) was calculated from the difference between potential evapotranspiration (from the Penman–Monteith method for grass) and rainfall. During the study period, the PSMD increased with time (Fig. 3).

Measurements of σ and θ_v on laboratory samples revealed different relationships for the two soil types (Fig. 4). Each showed a significant ($p < 0.001$) positive linear regression be-

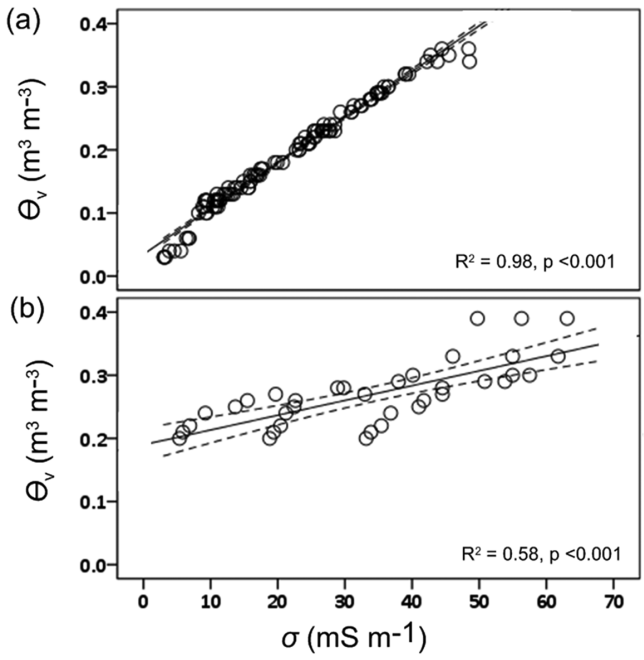

Fig. 4. Measurements of volumetric soil moisture content (θ_v) and soil electrical conductivity (σ) on soil cores extracted from (a) Butt Close and (b) Warren Field sites. The solid line shows the linear regression best estimate, the dashed line show 95% confidence intervals of the regression.

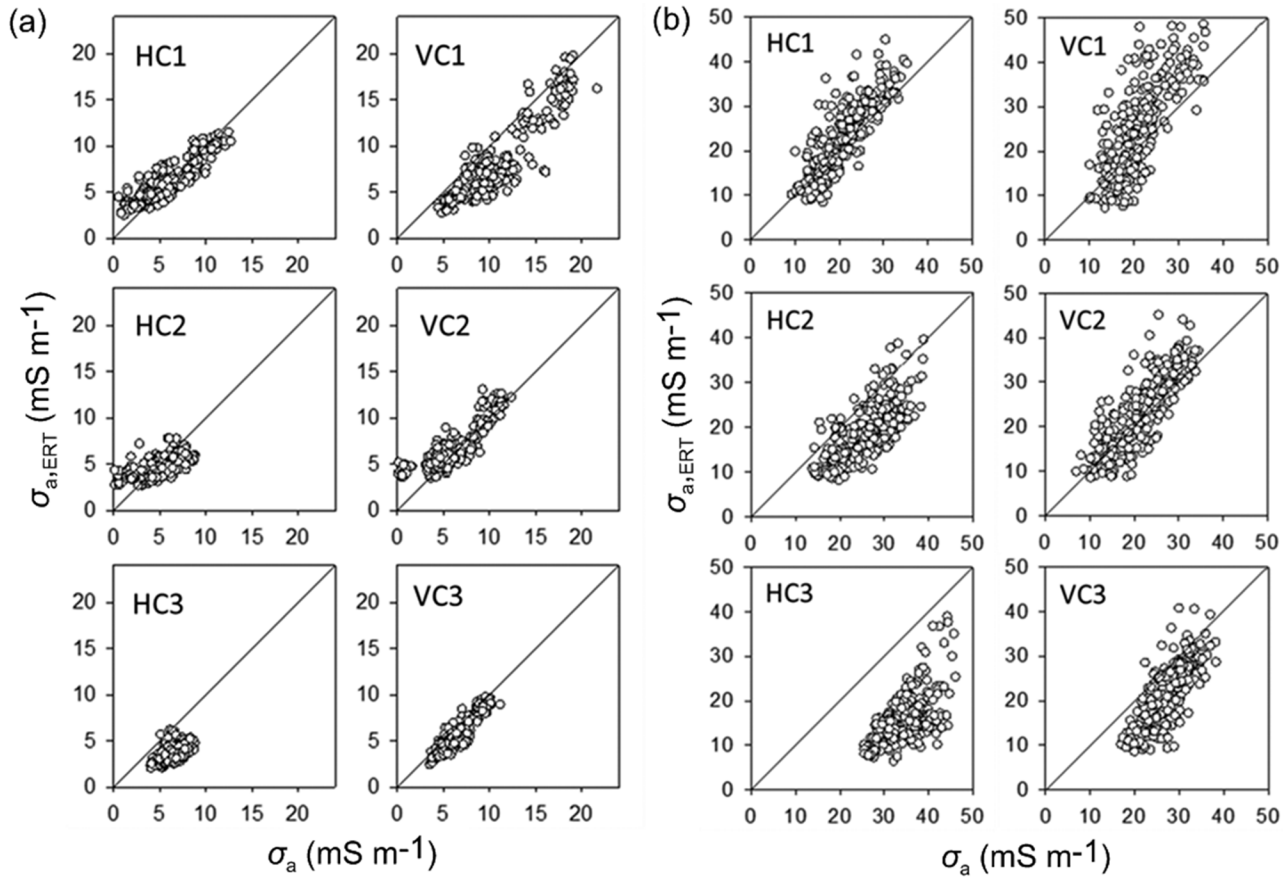

Fig. 5. Comparison of predicted ($\sigma_{a,ERT}$) and measured (σ_a) apparent electrical conductivities for the various CMD Mini-Explorer configurations of receivers (1–3) in horizontal coplanar (HC) and vertical coplanar (VC) modes for (a) Butt Close and (b) Warren field. The predicted values were computed from electrical resistivity tomography (ERT) data with Eq. [1–3] and σ–depth profiles determined from ERT inverse models. A 1:1 line is shown in each plot.

tween θ_v and σ within the limits of the pressure vessel (maximum 450 kPa). More scatter was evident in the data from the Warren Field samples. The data from the clay-rich Warren Field soil had a smaller slope than that from the sandy Butt Close soil. Thus, for a given change in θ_g at each site, the change in σ will be greater at the Warren Field site.

Predicting Electromagnetic Induction Data from Soil Profile Conductivities Measured with Electrical Resistivity Tomography

The six regressions between the EMI data predicted from ERT measurements and those measured are shown in Fig. 5 for each site. Grouped regression indicated that separate fits are needed for each of the coil configurations ($P < 0.001$). All of these relationships are statistically significant ($P < 0.001$), but the percentage of the variance accounted for varies between 34 and 83% (Table 2). The better agreements are generally found on the loamy sand site (Butt Close). The poorest agreement is on the more conductive sandy clay loam (Warren Field) with measurements obtained with a horizontal coplanar mode and a 1.18 m coil separation. This configuration is sensitive to greater depths (see Fig. 2). This is consistent with the regressions of Lavoué et al. (2010). The development of shrinkage cracks in the sandy clay loam may be in part responsible for the greater scatter for the Warren Field site; such cracks have been shown to adversely affect the performance of ERT (Ackerson et al., 2014).

We used the correlations shown in Fig. 5 to adjust the six EMI conductivity measurements before they were used in the inversion routine. This allows the quantitative use of EMI for mapping electrical conductivity (Lavoué et al., 2010). However, we do note that the agreement between predicted and measured EMI conductivities in Fig. 5 is close to the 1:1 line with the exception of HC3 on the sandy clay loam (Warren Field).

Table 2. Linear regression analysis of calculated apparent electrical conductivity ($\sigma_{a,ERT}$) from electrical resistivity tomography data to measured apparent electrical conductivity (σ_a) from the Mini-Explorer electromagnetic induction instrument for Butt Close and Warren Field site data. Results shown are for the six different coil configurations. The percentage of variance accounted for and the degrees of freedom are shown.

		$\sigma_{a,ERT}$ and σ_a regression analysis					
Site	Parameter	VC1	VC2	VC3	HC1	HC2	HC3
Butt Close	df	262	238	262	262	250	262
	variance, %	81	44	83	79	40	38
Warren Field	df	787	790	790	790	790	790
	variance, %	51	63	61	72	52	34

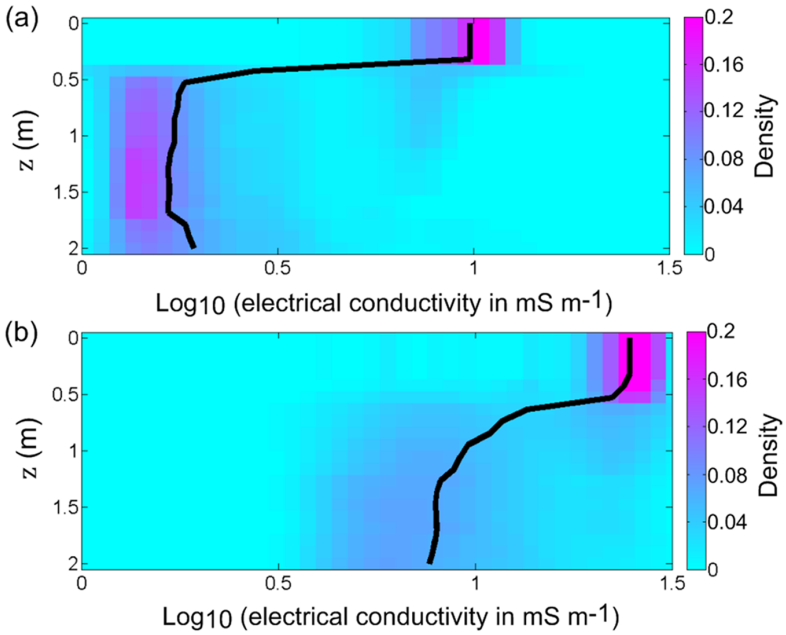

Fig. 6. An example of an inversion output of electromagnetic induction (EMI) data for (a) Butt Close and (b) Warren Field. The solid black line shows the posterior median electrical conductivity $\sigma(z)$. The color scale indicates the density of the estimated models, calculated by discretizing the estimated models at 10-cm depth intervals (z), then calculating the normalized histogram at z.

Electrical Conductivity Profiles Predicted from Inversion of Electromagnetic Induction Data

Examples of typical $\sigma(z)$ profiles obtained from the inversion of Butt Close and Warren Field EMI data (26 June 2014) are shown in Fig. 6 following JafarGandomi and Binley (2013). In this example, we show the estimated a posteriori median $\sigma(z)$ models, the 98% confidence intervals of the posteriori distributions. The probability of estimated models is calculated using the McMC algorithm by discretizing the estimated models at 10-cm depth intervals and then calculating the normalized histogram per depth interval (i.e., density of values per 10-cm depth interval). Figure 6 shows the density of predicted σ values per 10-cm depth interval in the chart color scale.

Our results show that σ decreased at depth at both sites, although θ_g at depth was greater than or similar to those at the surface. This was particularly marked at Butt Close, where at depth (deeper than 40 cm) the soil is almost pure sand. On this site, the lower σ at deep layers was almost certainly due to the lack of silt and clay (which would contribute to a surface conductivity). The change in σ with depth at Warren Field was much smaller than it was at Butt Close. However, lower σ in deeper layers at Warren Field is consistent with a lower porosity, despite a similar θ_g. These profile σ data give a clear illustration of the difficulty of simply relating σ to θ_g.

Interpretation of Changes in Electrical Conductivity Due to Water Uptake by Wheat

The actual relationship between σ and θ_g is different for the two soil types on Butt Close and Warren Field (Fig. 4). By assuming that the change with time in bulk electrical conductivity ($\Delta\sigma$) is dominated by the effects of θ_g, differences in σ between 16 May and later dates reflect the change in θ_g. In Fig. 7, comparisons are made between changes in σ and changes in θ_g. From these observations it can be seen that there is greater agreement between changes in σ and changes in θ_g for the earlier dates and that the agreement is better for the loamy sand soil at

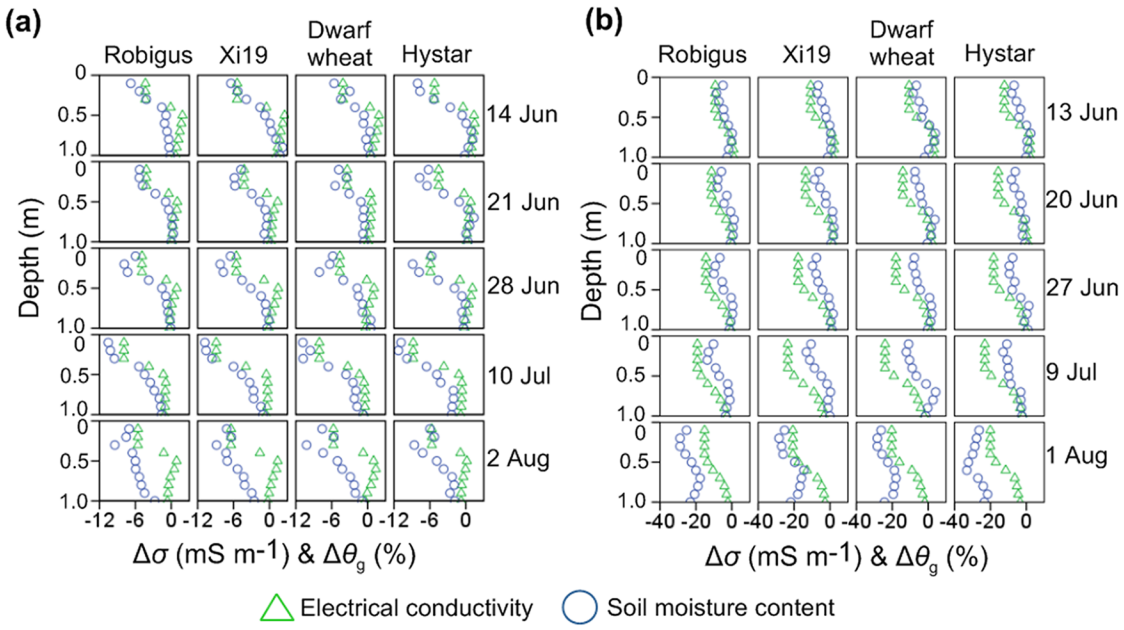

Fig. 7. The change in electrical conductivity ($\Delta\sigma$) determined from electromagnetic induction (EMI) measurements and the change in gravimetric soil moisture content ($\Delta\theta_g$) plotted against depth for (a) Butt Close and (b) Warren Field plots sown with Robigus, Xi19, Dwarf wheat, and Hystar wheat genotypes (n = 4). Reference dates for the sites are 16 May 2013 and 14 May 2013 for Butt Close and Warren Field, respectively.

Butt Close (Fig. 7a) than it is for the clay loam at Warren Field (Fig. 7b). The use of changes in σ to indicate changes in θ_g is predicated on the assumption that a change in σ is simply due to a change in the volume of fluid. The better agreement between changes in σ and changes in θ_g at early dates and more generally on the sandier site at Butt Close (Table 3) may possibly be related to the effect of the conductivity of the pore water, which is likely to be greater on soils that are drier or have a greater clay content (Hilhorst, 2000). Thus in dry or clay-rich soils, changes in bulk σ, measured by EMI, may be confounded by increased pore water conductivity and less closely associated with changes in θ_g. Nevertheless, Fig. 8 and Table 3 support the approach of using changes in σ determined from EMI inversion procedures to explore changes in θ_g with depth, although we did not find a single calibration that applied to all data sets in Fig. 7.

The change in Δσ with depth is different at the two sites. At Butt Close (Fig. 8a), a drop in σ during the measurement period is apparent in the upper 0.6 m, most notably in the top 0.3 m. This is consistent with more intense surface drying on this site due to root growth restricted to the surface layers as a result of the cemented layer 40 cm below the surface (Whalley et al., 2008). At Butt Close, the relationship between the change in σ and depth was not monotonic, and there was an anomaly at a depth of approximately 0.5 m, possibly due to the cemented layer. In contrast, at Warren Field the relationships between Δσ and depth (Fig. 8b) were smooth and monotonic and lend themselves to curve fitting with

$$\Delta\sigma(z) = A + \frac{C}{1+\exp\left[-b\left(z-M\right)\right]} \qquad [4]$$

Table 3. The percentage of variance accounted for in the regression between the change in electrical conductivity and change in gravimetric water content plotted in Fig. 7. In all cases the fit to the data as significant at $p < 0.001$.

Date	Variance accounted for
	%
Butt Close	
14 June	82.8
21 June	82.7
28 June	79.4
10 July	93.4
2 Aug.	36.7
Warren Field	
13 June	69.9
20 June	69.5
27 June	83.8
9 July	71.8
1 Aug.	35.9

where *A*, *b*, *C*, and *M* are fitting parameters; *A* and *C* are the asymptotes of the S curve, *b* controls the steepness of the transition between these asymptotes, and *M* defines the depth of inflection in the soil profile. This type of curve is consistent with the saturation depth curves modeled by Roose and Fowler (2004) for the water-limited condition. The value of *M* provides a useful parameter to make simple comparisons of the drying depth within the profile (Fig. 8c). During the growth period, the depth of water extraction by roots increases (Gregory et al., 2013). This is in agreement with an increase in *M* values with time, as plotted in Fig. 8c for the four wheat genotypes. Although the potential soil moisture deficit (for grass) continues to increase beyond July, the *M* values decrease (suggesting that the soil profile is wetting),

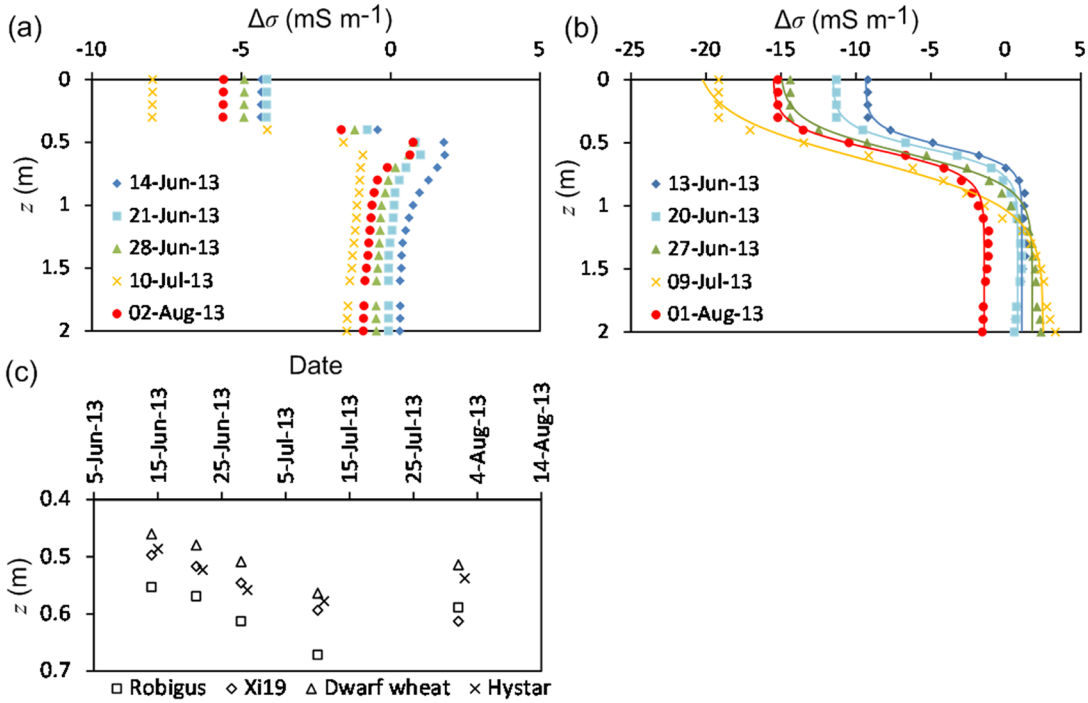

Fig. 8. The change in electrical conductivity (Δσ) for (a) Butt Close and (b) Warren Field relative to reference dates 16 May 2013 and 14 May 2013, respectively, as a function of depth, and (c) the depth of the inflection point (*M* in Eq. [4]) for the curves fitted to the data from Warren Field for Hystar, Robigus, Xi19, and Dwarf wheat genotypes plotted against date.

which is consistent with crop senescence and a lower demand for water. The Dwarf wheat was the least effective at deep water uptake, which is probably due to a shallower rooting depth.

CONCLUSIONS

Using EMI measurements, we show that changes in conductivity are consistent with measured changes in soil water content in the root zone of wheat. On a sandy clay loam, the changes in conductivity were consistent with expected soil water profiles for water-limited conditions and also consistent with the progress of the crop from a vegetative stage, with high water demand, to a senesced condition with low water uptake. Differences in the inferred depth of water uptake were observed among the four wheat genotypes studied. On the loamy sand soil, with a cemented layer at a depth of approximately 0.4 m, water uptake appeared to be confined to the surface layers and controlled by soil lithological characteristics. On this site, drawing inferences about differences between root water uptake between wheat genotypes or the effect of growth stage is not possible, although the value of EMI as a tool to investigate soil–crop interactions is apparent.

ACKNOWLEDGMENTS

This study was funded by the BBSRC Crop Improvement Research Club as part of project BB/J01950X/1. We would like to thank Rhys Ashton, Colin Webster, Rodger White, and Woburn Farm of Rothamsted Research. Richard Whalley and Chris Watts are funded by the 20:20® project at Rothamsted Research. We further acknowledge the following companies with regard to the wheat genotypes used: Saaten-Union Gmbh, Germany; Limagrain UK Ltd.; and KWS UK Ltd. Thanks to Arash JafarGandomi, formerly Lancaster University, for his help in compiling the inversion algorithm code.

REFERENCES

Ackerson, J.P., C.L.S. Morgan, M.E. Everett, and K.J. McInnes. 2014. The role of water content in electrical resistivity tomography of a Vertisol. Soil Sci. Soc. Am. J. 78:1552–1562. doi:10.2136/sssaj2014.01.0032

Araus, J.L., and J.E. Cairns. 2014. Field high-throughput phenotyping: The new crop breeding frontier. Trends Plant Sci. 19:52–61. doi:10.1016/j.tplants.2013.09.008

Archie, G.E. 1942. The electrical resistivity log as an aid in determining some reservoir characteristics. Trans. Am. Inst. Min. Metall. Pet. Eng. 146:54–61.

Bengough, A.G., B.M. McKenzie, P.D. Hallett, and T.A. Valentine. 2011. Root elongation, water stress, and mechanical impedance: A review of limiting stresses and beneficial root tip traits. J. Exp. Bot. 62:59–68. doi:10.1093/jxb/erq350

Binley, A. 2013. R2 version 2.7a February 2013. Lancaster Environ. Ctr., Lancaster Univ., Lancaster, UK. http://www.es.lancs.ac.uk/people/amb/Freeware/R2/R2.htm

Binley, A., and A. Kemna. 2005. DC resistivity and induced polarization methods. In: Y. Rubin and S.S. Hubbard, editors, Hydrogeophysics. Springer, Dordrecht, the Netherlands. p. 129–156.

Brevik, E.C., T.E. Fenton, and A. Lazari. 2006. Soil electrical conductivity as a function of soil water content and implications for soil mapping. Precis. Agric. 7:393–404. doi:10.1007/s11119-006-9021-x

Callegary, J.B., T.P.A. Ferré, and R.W. Groom. 2007. Vertical spatial sensitivity and exploration depth of low-induction-number electromagnetic-induction instruments. Vadose Zone J. 6:158–167. doi:10.2136/vzj2006.0120

Campbell, R.B., C.A. Bower, L.A. Richards. 1949. Change of electrical conductivity with temperature and the relation of osmotic pressure to electrical conductivity and ion concentration for soil extracts. Soil Sci. Soc. Am. Proc. 13:66–69. doi:10.2136/sssaj1949.036159950013000C0010x

Cassiani, G., N. Ursino, R. Deiana, G. Vignoli, J. Boaga, M. Rossi, et al. 2012. Noninvasive monitoring of soil static characteristics and dynamic states: A case study highlighting vegetation effects on agricultural land. Vadose Zone J. 11(3). doi:10.2136/vzj2011.0195

Corwin, D.L., and S.M. Lesch. 2005. Apparent soil electrical conductivity measurements in agriculture. Comput. Electron. Agric. 46:11–43. doi:10.1016/j.compag.2004.10.005

Dodd, I.C., W.R. Whalley, E.S. Ober, and M.A.J. Parry. 2011. Genetic and management approaches to boost UK wheat yields by ameliorating water deficits. J. Exp. Bot. 62:5241–5248. doi:10.1093/jxb/err242

Furman, A., A. Arnon-Zur, and S. Assouline. 2013. Electrical resistivity tomography of the root zone. In: S.H. Anderson and J.W. Hopmans, editors, Soil–water–root processes: Advances in tomography and imaging. SSSA Spec. Publ. 61. SSSA, Madison, WI. p. 221–242. doi:10.2136/sssaspecpub61.c11

Gregory, P.J., C.J. Atkinson, A.G. Bengough, M.A. Else, F. Fernández-Fernández, R.J. Harrison, and S. Schmidt. 2013. Contributions of roots and rootstocks to sustainable, intensified crop production. J. Exp. Bot. 64:1209–1222. doi:10.1093/jxb/ers385

Hilhorst, M.A. 2000. A pore water conductivity sensor. Soil Sci. Soc. Am. J. 64:1922–1925. doi:10.2136/sssaj2000.6461922x

JafarGandomi, A., and A. Binley. 2013. A Bayesian trans-dimensional approach for the fusion of multiple geophysical datasets. J. Appl. Geophys. 96:38–54. doi:10.1016/j.jappgeo.2013.06.004

Lavoué, F., J. van der Kruk, J. Rings, F. André, D. Moghadas, J.A. Huisman, et al. 2010. Electromagnetic induction calibration using apparent electrical conductivity modelling based on electrical resistivity tomography. Near Surface Geophys. 8:553–561. doi:10.3997/1873-0604.2010037

McNeill, D.J. 1980. Electromagnetic terrain conductivity measurement at low induction numbers. Tech. Note TN-6. Geonics Ltd., Mississauga, ON, Canada.

Mester, A., J. van der Kruk, E. Zimmermann, and H. Vereecken. 2011. Quantitative two-layer conductivity inversion of multi-configuration electromagnetic induction measurements. Vadose Zone J. 10:1319–1330. doi:10.2136/vzj2011.0035

Parasnis, D.S. 1988. Reciprocity theorems in geoelectric and geoelectromagnetic work. Geoexploration 25:177–198. doi:10.1016/0016-7142(88)90014-2

Roose, T., and A.C. Fowler. 2004. A model for water uptake by plant roots. J. Theor. Biol. 228:155–171. doi:10.1016/j.jtbi.2003.12.012

Srayeddin, I., and C. Doussan. 2009. Estimation of the spatial variability of root water uptake of maize and sorghum at the field scale by electrical resistivity tomography. Plant Soil 319:185–207. doi:10.1007/s11104-008-9860-5

Vanderborght, J., J.A. Huisman J. van der Kruk, and H. Vereecken. 2013. Geophysical methods for field-scale imaging of root zone properties and processes. In: S.H. Anderson and J.W. Hopmans, editors, Soil–water–root processes: Advances in tomography and imaging. SSSA Spec. Publ. 61. SSSA, Madison, WI. p. 247–282. doi:10.2136/sssaspecpub61.c12

Vereecken, H., J.A. Huisman, Y. Pachepsky, C. Montzka, J. van der Kruk, H. Bogena, et al. 2014. On the spatio-temporal dynamics of soil moisture at the field scale. J. Hydrol. 516:76–96. doi:10.1016/j.jhydrol.2013.11.061

von Hebel, C., S. Rudolph, A. Mester, J.A. Huisman, P. Kumbhar, H. Vereecken, and J. van der Kruk. 2014. Three-dimensional imaging of subsurface structural patterns using quantitative large-scale multiconfiguration electromagnetic induction data. Water Resour. Res. 50:2732–2748. doi:10.1002/2013WR014864

Whalley, W.R., M. Jenkins, and K. Attenborough. 2012. The velocity of shear waves in unsaturated soil. Soil Tillage Res. 125:30–37. doi:10.1016/j.still.2012.05.013

Whalley, W.R., C.W. Watts, P.J. Gregory, S.J. Mooney, L.J. Clark, and A.P. Whitmore. 2008. The effect of soil strength on the yield of wheat. Plant Soil 306:237–247. doi:10.1007/s11104-008-9577-5